IET Renewable Power Generation

Research Article

Probabilistic active distribution network equivalence with correlated uncertain injections for grid analysis

ISSN 1752-1416
Received on 19th September 2019
Revised 4th April 2020
Accepted on 15th May 2020
E-First on 17th July 2020
doi: 10.1049/iet-rpg.2019.1068
www.ietdl.org

Bin Huang[1,2], Zhigang Li[1] ✉, Jiehui Zheng[1], Q.H. Wu[1]

[1]*School of Electric Power Engineering, South China University of Technology, Guangzhou, 510640, People's Republic of China*
[2]*Department of Electrical and Computer Engineering, Southern Methodist University, Dallas, USA*
✉ *E-mail: lizg16@scut.edu.cn*

Abstract: Equivalent modelling for active distribution networks (ADNs) is essential for improving the efficiency of analysing transmission networks. Current equivalent modelling methods for ADNs neglect the probabilistic characteristics of renewable energy sources (RESs) and loads. To address this issue, this study proposes a probabilistic equivalent modelling method (PEMM) for ADNs considering the uncertainty of RESs and loads. The uncertainty of the RESs and loads is transferred to the equivalent boundary bus injection using the properties of cumulant and power transfer matrices. The PEMM is extended to incorporate the correlations of RESs through an orthogonal transformation. A sampling method using the Gaussian copula function is employed to generate the correlated samples and the joint cumulants, providing the input data for the PEMM. The comparative results of the case studies on two different test systems demonstrate the effectiveness of the PEMM. The equivalent model developed in this study is a practical solution for analysing the transmission network efficiently and taking the uncertainty of RESs and loads in the ADNs into account simultaneously.

1 Introduction

Because of the increasing appeal of the utilisation of clean energy, large-scale renewable energy sources (RESs) are being integrated into distribution networks [1–3]. Currently, the conventional distribution networks are gradually becoming active distribution networks (ADNs), which may supply surplus power to the transmission network when RESs are abundant. Hence, the analysis of coupled transmission and distribution systems (CTDSs) must consider the impact of RESs. From the perspective of transmission system operators (TSOs), it is impractical and unnecessary to analyse the transmission side using the detailed model of ADNs for two reasons. First, the scale and complexity of ADNs impair the efficiency of the analysis procedure. Second, TSOs and distribution system operators (DSOs) usually function independently, which means that detailed information about them is commercially sensitive and not transparent to each other. As an essential tool to analyse transmission networks considering the impact of RESs, equivalent methods for ADNs have recently attracted the attention of researchers. The main goal of these equivalent methods is to construct an equivalent model for ADNs that can preserve the behaviours of the ADN while keeping the structure and mathematical model as simple as possible.

The conventional (passive) distribution network usually consists of loads, lines, distribution transformers, regulators, switches shunt capacitors etc. In the previous works, the whole model of the passive distribution network is assumed to be deterministic when the equivalent model is needed. Under this context, a deterministic equivalent model is developed, which includes the deterministic equivalent load, equivalent boundary shunt branch and sometimes deterministic equivalent generators if the distributed generators (DGs) are considered [4]. The equivalent model derived in a deterministic manner can guarantee the consistency of the load flow before and after equivalence.

However, the conventional equivalent technique of the passive distribution network is not appropriate for the ADNs anymore because the ADNs are characterised by the penetration of RESs, and the generation of RESs and loads is inherently stochastic [2, 3]. The modelling of renewable power generation is critical to the equivalence of ADNs. To conduct the dynamic analysis, [5–7] use an equivalent converter-connected synchronous generator to represent the DGs in an ADN. In [8], photovoltaic (PV) generation systems embedded with voltage support schemes in an ADN are aggregated into a separate equivalent PV generator that preserves the voltage support schemes. In [9], the equivalent model for DGs is derived using a numerical approach, in which the reactive power output and the inverter power loss of the DGs are considered. The authors in [4, 10] adopt an equivalent generator to represent the DGs in ADNs, and the nodes with DGs connected in the ADN are regarded as either PQ nodes or PV nodes. The aforementioned literatures [4–10] ignore the uncertainty of the RES-type DGs. When analysing the transmission network, it is necessary to take the uncertainties from the ADNs into account, because a transmission network is usually connected with numerous ADNs and ADN is one of the main sources of uncertainty from the perspective of the transmission network. These uncertainties will impact the secure and economic operation of the bulk power system significantly. For example, in terms of the economic dispatch, neglecting the uncertainty of RESs may result in an untrustworthy operation schedule, and thus, operators may have to deploy excessive reserve capacity [11]. Moreover, to obtain a practical and feasible solution for the long-term planning and congestion management of the bulk power system, it is imperative for TSOs to incorporate the uncertainty from ADNs. When examining the status of power grids, the TSOs must monitor and evaluate the level of uncertainty of the system to ensure stability and reliability. Under such context, it is imperative to develop an equivalent model for ADNs which not only can ensure the consistency of the load flow but also the probabilistic characteristic.

In addition to the uncertain property, another critical feature of RESs is the correlation. Owing to the fact that the regional scope of ADNs is usually small and because the meteorological conditions within ADNs are similar, the wind power generation in different wind farms (WFs) in an ADN is correlated [12], as the PV generation between different PV plants. Ignoring the correlation can lead to biases in the analysis results for a system, resulting in higher operating costs and higher risks to the stability of the power system [13]. Hence, an equivalent model for ADNs should consider the correlations among RESs. Usaola [14] used the Cholesky decomposition to generate the correlated variables representing linear correlations. Xie *et al*. [12] used the copula function to describe non-linear correlations. However, when using the copula function to handle the correlations, few references investigate the derivation of the joint cumulants, which are the essential quantities of the joint probability distribution.

To summarise, few studies have considered the uncertainty of RESs when developing the equivalent models for ADNs even though the uncertainty of RESs is essential in the analysis and optimisation of CTDS. In addition, the correlations among RESs are seldom discussed in the current equivalent modelling methods. Initially, the computational intractability and the independent operation between DSOs and TSOs lead to the development of the equivalent modelling techniques of the distribution system. Then the trend of the transformation of the passive distribution system to ADNs and the increasing penetration level of RESs in the level of ADNs together necessitates developing a novel equivalent method that can address the severe uncertainty. To this end, the emphasis of this paper lies in developing the probabilistic equivalent modelling method (PEMM) for ADN, which considers the correlated uncertain power injections caused by RES and load. As shown in Fig. (b), the correlated uncertain power injections are shifted to the boundary via quantitative analysis of the power flow equations of the ADNs which incorporate PV plants and WFs. PEMM has resulted in a practical solution for analysing the transmission network efficiently and considering the uncertainty in the ADNs simultaneously. More specifically, one of the application scenarios is the steady-state analysis of the transmission grid, such as the probabilistic load flow (PLF) calculation. A distinct advantage of PEMM is that it can accelerate the PLF calculation on the transmission grid by getting rid of using the detailed model of ADN. Another advantage of PEMM is that it can be conducted by DSOs independently, eliminating the need for sharing the commercially sensitive operation information with TSOs.

The contributions of this paper are summarised as follows:

(i) A PEMM is proposed to obtain an equivalent model considering the probabilistic features pertaining to RESs for ADNs. The uncertain property of RESs is aggregated to the boundary bus using the properties of the cumulant and the power transfer matrices derived from the nodal voltage equations. The PEMM only relies on the information of ADNs and thus the equivalent model can be developed by the DSOs independently. Under this context, the PEMM can facilitate the coordination between DSOs and TSOs and improve the reliability of the transmission systems by providing a solution for TSOs to consider the uncertainty from ADNs without compromising the efficiency of analysis.
(ii) The formulation of PEMM is extended to incorporate the correlated power injections through an orthogonal transformation, which can extend the scope of PEMMs to the equivalent modelling of ADNs with the correlated RESs integrated.
(iii) The performance of the proposed PEMM is demonstrated by comparing it with the loss ratio (LR) method on two different test systems. The case studies verify that using the PEMM can accelerate the analysis and calculation toward the transmission system without simultaneously compromising the accuracy.

The remainder of this paper is organised as follows. Power injections with uncertainty in ADNs are formulated in Section 2. In Section 3, the PEMM for ADNs is proposed and extended to incorporate the correlated power generation of RESs. A sampling method for generating the correlated samples and the joint cumulants using the copula function is also described in Section 3. In Section 4, case studies on two different test systems are performed to evaluate the accuracy and efficiency of the proposed PEMM. Finally, conclusions and future work are given in Section 5.

2 Modelling of uncertain power injections in ADNs

An ADN is characterised by the high penetration of RESs, which are inherently stochastic because of the environmental conditions. Moreover, the loads in ADNs are uncertain because of prediction errors and their inherent stochastic nature. In this section, the uncertainty of the power injection of ADN is described. The model of PVs is presented first, followed by the model for wind power and load.

2.1 Model of PVs

An ADN is typically equipped with PV plants to supply usable solar power. The beta distribution is used to model the uncertainty of solar irradiance [15]:

$$f_r(r)=\begin{cases}\dfrac{\Gamma(\alpha+\beta)}{\Gamma(\alpha)+\Gamma(\beta)} & \left(\dfrac{r}{r_{\max}}\right)^{\alpha-1}\left(1-\dfrac{r}{r_{\max}}\right)^{\beta-1} \\ & 0\le r\le r_{\max},\ \alpha\ge 0,\beta\ge 0\text{'} \\ 0 & r\le 0 \quad \text{or} \quad r\ge r_{\max}\end{cases} \tag{1}$$

where r and $r_{\max}$ are the solar irradiance and maximum solar irradiance, respectively; α and β are the function parameters and Γ represents the Γ function.

Accordingly, the probability density function (PDF) of the active power output of a PV plant is formulated as

$$f_{\rm pv}(P_{\rm pv})=\frac{\Gamma(\alpha+\beta)}{\Gamma(\alpha)+\Gamma(\beta)}\left(\frac{P_{\rm pv}}{P_{\rm pv,max}}\right)^{\alpha-1}\left(1-\frac{P_{\rm pv}}{P_{\rm pv,max}}\right)^{\beta-1}, \tag{2}$$

$P_{\rm pv,max}$ is the maximum active power output of the PV plant:

$$P_{\rm pv,max}=A\eta_{\rm pv}r_{\max}, \tag{3}$$

where $\eta_{\rm pv}$ is the comprehensive conversion efficiency of the PV plant and A is the area of the PV cells within a PV plant.

2.2 Model of wind power

The Weibull distribution is commonly used to describe the probabilistic nature of wind speeds [12]:

$$f_{\rm w}(x)=\begin{cases}\dfrac{k}{\lambda}\left(\dfrac{x}{\lambda}\right)^{k-1}\exp\left(-\left(\dfrac{x}{\lambda}\right)^{k}\right) & x\ge 0 \\ 0 & x\le 0\end{cases}, \tag{4}$$

where x is the wind speed, k is the shape parameter of the distribution and λ is the scale parameter of the distribution.

The relationship between the wind speed and the output power of a WF is formulated as [12]

$$P_{\rm w}(v)=\begin{cases}0, & v\le v_{\rm ci}, v\ge v_{\rm co} \\ P_{\rm N}, & v_{\rm N}\le v\le v_{\rm co} \\ g(v), & v_{\rm ci}\le v\le v_{\rm N}\end{cases}, \tag{5}$$

where $v_{\rm ci}$, $v_{\rm co}$ and $v_{\rm N}$ are the cut-in, cut-out and nominal wind speed, respectively; $g(v)$ is a function that describes the relationship between the power output and the wind speed in the interval of wind speed $[v_{\rm ci}, v_{\rm N}]$ and can be expressed as

$$g(v)=\frac{1}{2}\pi\rho C_{\rm p}(\lambda,\beta)R^2v^3, \tag{6}$$

in which ρ is the air density (typically 1.25 km/m^3), β is the pitch angle (in degrees), R is the blade radius (in metres) and $C_{\rm p}(\lambda,\beta)$ is the wind-turbine power coefficient.

Supposing a WF adopts the control strategy of constant power factor, the reactive power generated by a WF can be calculated as

$$Q_{\rm w}=P_{\rm w}\sqrt{1-\cos^2\varphi}/\cos\varphi, \tag{7}$$

where $\cos\varphi$ is the power factor of the WF.

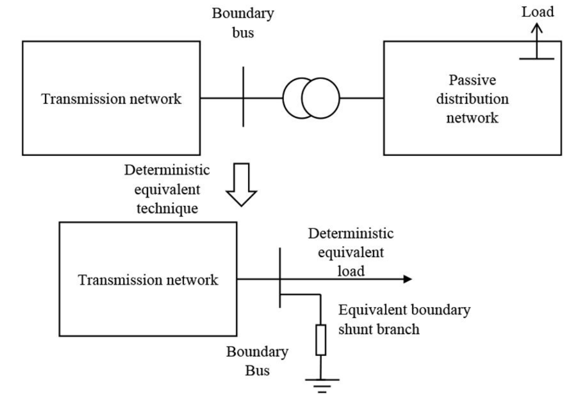

Fig. 1 *Conventional deterministic equivalent technique*

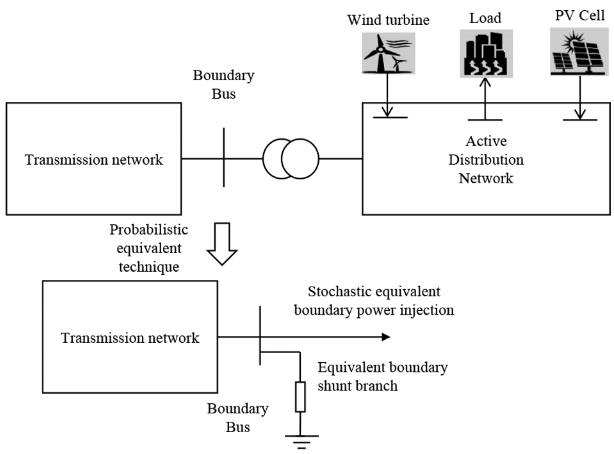

Fig. 2 *Illustrative example of the PEMM*

2.3 Load

Considering the time-varying and uncertain nature of loads, the normal distribution is commonly used to describe the active power load uncertainty [15, 16]:

$$f_1(P_1) = \exp\left[-\frac{(P_1 - \mu_{P_1})^2}{2\sigma_{P_1}^2}\right] / \sqrt{2\pi}\sigma_{P_1}, \tag{8}$$

where $f(P_1)$ is the PDF of the active power load, and μ_{P_1} and σ_{P_1} are the mean and standard derivation of the active power load, respectively.

The PDF of the reactive power load can be similarly derived.

3 Probabilistic equivalent modelling of ADNs

Generally, the transmission network and distribution networks are interconnected via a boundary bus, which is the physical distribution substation. An illustrative example of the conventional deterministic equivalent technique for the passive distribution network is depicted in Fig. 1. The assumption behind this technique is that all components of the distribution system are deterministic. By contrast, the PEMM proposed in this paper incorporates the uncertainties caused by the RESs and loads.

As shown in Fig. 2, by replacing the ADN with the stochastic equivalent boundary power injection and the equivalent boundary shunt branch, the primary goal of the PEMM is to accelerate the analysis of the transmission system. The stochastic equivalent boundary power injection can represent the uncertain power injections and the power loss in the ADNs. The equivalent boundary shunt branch can represent the shunt components in the ADNs. The equivalent model derived from the PEMM can retain the consistency of the load flow as well as that of the probabilistic nature in ADNs before and after equivalence.

In this section, we first introduce the derivation of power transfer matrices, which are the basic components of the proposed PEMM. Subsequently, the proposed PEMM is extended to incorporate the correlation. The copula function, which is utilised to characterise the correlation between the RES and the inverse transform sampling-based method is used to derive the joint cumulants of power injections.

3.1 Power transfer matrices

The nodal voltage equations of the CTDS can be expressed in matrix form:

$$\begin{bmatrix} \boldsymbol{Y}_{\rm EE} & \boldsymbol{Y}_{\rm EB} & \\ \boldsymbol{Y}_{\rm BE} & \boldsymbol{Y}_{\rm BB} & \boldsymbol{Y}_{\rm BI} \\ & \boldsymbol{Y}_{\rm IB} & \boldsymbol{Y}_{\rm II} \end{bmatrix} \begin{bmatrix} \dot{\boldsymbol{V}}_{\rm E} \\ \dot{\boldsymbol{V}}_{\rm B} \\ \dot{\boldsymbol{V}}_{\rm I} \end{bmatrix} = \begin{bmatrix} \dot{\boldsymbol{I}}_{\rm E} \\ \dot{\boldsymbol{I}}_{\rm B} \\ \dot{\boldsymbol{I}}_{\rm I} \end{bmatrix}, \tag{9}$$

where $\boldsymbol{Y}$ is the bus admittance matrix, $\dot{\boldsymbol{V}}$ is the nodal voltage vector, $\dot{\boldsymbol{I}}$ is the nodal current injection vector and the subscripts E, B, I denote the elements of the matrix and the vector corresponding to the buses of the ADN, the boundary buses and the buses of the transmission network, respectively.

By performing Gaussian elimination on (9) to eliminate $\dot{\boldsymbol{V}}_{\rm E}$ and transforming the nodal current injection into the nodal power injection, the nodal voltage equations of the boundary buses in the equivalent network can be expressed as

$$\begin{aligned} &(\boldsymbol{Y}_{\rm BB} - \boldsymbol{Y}_{\rm BE}\boldsymbol{Y}_{\rm EE}^{-1}\boldsymbol{Y}_{\rm EB})\dot{\boldsymbol{V}}_{\rm B} + \boldsymbol{Y}_{\rm BI}\dot{\boldsymbol{V}}_{\rm I} = \\ &(\mathrm{diag}[\dot{\boldsymbol{V}}_{\rm B}]^{-1})^{*}\dot{\boldsymbol{S}}_{\rm B}^{*} - \boldsymbol{Y}_{\rm BE}\boldsymbol{Y}_{\rm EE}^{-1}(\mathrm{diag}[\dot{\boldsymbol{V}}_{\rm E}]^{-1})^{*}\dot{\boldsymbol{S}}_{\rm E}^{*}, \end{aligned} \tag{10}$$

where $\dot{\boldsymbol{S}}$ is the nodal power injection, $()^{*}$ denotes the conjugate operator and diag[ ] is the diagonal operator.

Derived from the right side of (10), the equivalent boundary power injection can be formulated as

$$\Delta\dot{\boldsymbol{S}}_{\rm B} = -\,\mathrm{diag}[\dot{\boldsymbol{V}}_{\rm B}]\boldsymbol{Y}_{\rm BE}\boldsymbol{Y}_{\rm EE}^{-1}\mathrm{diag}[\dot{\boldsymbol{V}}_{\rm E}]^{-1}\dot{\boldsymbol{S}}_{\rm E}. \tag{11}$$

$\Delta\dot{\boldsymbol{S}}_{\rm B}$ is determined jointly by $\boldsymbol{Y}_{\rm BE}\boldsymbol{Y}_{\rm EE}^{-1}$, $\dot{\boldsymbol{V}}_{\rm B}$, $\dot{\boldsymbol{V}}_{\rm E}$ and $\dot{\boldsymbol{S}}_{\rm E}$ at a specific operating point. Assuming that $\boldsymbol{Y}_{\rm BE}\boldsymbol{Y}_{\rm EE}^{-1}$, $\dot{\boldsymbol{V}}_{\rm B}$ and $\dot{\boldsymbol{V}}_{\rm E}$ are constants at a basic operating point, the equivalent boundary power injections are approximately linear to the power injections in ADNs in decoupled forms:

$$\Delta\boldsymbol{P}_{\rm B} = \boldsymbol{E}_{\rm P}\boldsymbol{P}_{\rm E} + \boldsymbol{E}_{\rm Q}\boldsymbol{Q}_{\rm E}, \tag{12}$$

$$\Delta\boldsymbol{Q}_{\rm B} = -\,\boldsymbol{E}_{\rm Q}\boldsymbol{P}_{\rm E} + \boldsymbol{E}_{\rm P}\boldsymbol{Q}_{\rm E}, \tag{13}$$

where $\boldsymbol{P}$ and $\boldsymbol{Q}$ are the active and reactive parts of the complex power injections, respectively. Equations (12) and (13) show the power transfer characteristics in the ADNs. $\boldsymbol{E}_{\rm P}$ and $\boldsymbol{E}_{\rm Q}$ are the power transfer matrices, which can be calculated by

$$\begin{aligned} \boldsymbol{E}_{\rm P} &= \boldsymbol{C}_{\rm B1}\mathrm{diag}(|\boldsymbol{V}_{\rm E}|)^{-2}\boldsymbol{V}_{\rm E,Re} + \boldsymbol{C}_{\rm B2}\mathrm{diag}(|\boldsymbol{V}_{\rm E}|)^{-2}\boldsymbol{V}_{\rm E,Im}, \\ \boldsymbol{E}_{\rm Q} &= \boldsymbol{C}_{\rm B1}\mathrm{diag}(|\boldsymbol{V}_{\rm E}|)^{-2}\boldsymbol{V}_{\rm E,Im} - \boldsymbol{C}_{\rm B2}\mathrm{diag}(|\boldsymbol{V}_{\rm E}|)^{-2}\boldsymbol{V}_{\rm E,Re}, \end{aligned} \tag{14}$$

$$\begin{aligned} \boldsymbol{C}_{\rm B1} &= \mathrm{diag}[\boldsymbol{V}_{\rm B,Re}](\boldsymbol{Y}_{\rm BE}\boldsymbol{Y}_{\rm EE}^{-1})_{\rm Re} - \mathrm{diag}[\boldsymbol{V}_{\rm B,Im}](\boldsymbol{Y}_{\rm BE}\boldsymbol{Y}_{\rm EE}^{-1})_{\rm Im}, \\ \boldsymbol{C}_{\rm B2} &= \mathrm{diag}[\boldsymbol{V}_{\rm B,Im}](\boldsymbol{Y}_{\rm BE}\boldsymbol{Y}_{\rm EE}^{-1})_{\rm Re} + \mathrm{diag}[\boldsymbol{V}_{\rm B,Re}](\boldsymbol{Y}_{\rm BE}\boldsymbol{Y}_{\rm EE}^{-1})_{\rm Im}, \end{aligned} \tag{15}$$

in which $(*)_{\rm Re}$ and $(*)_{\rm Im}$ represent the real and imaginary part of $(*)$, respectively, and $|*|$ denotes the magnitude of a complex number.

With (10), the certain equivalent boundary power injection and the equivalent boundary shunt branch in Fig. 2 can be calculated, thereby building the Ward-type equivalent models for ADNs. Although the Ward-type equivalent models can guarantee the consistency of the load flow before and after the equivalence, they are not able to take the uncertainty of ADNs into consideration. Hence, they are not suitable for the equivalent modelling of ADNs with uncertain power injections.

Equation (10) is one kind of the Ward-type equivalence. The Ward-type equivalence could cause errors when $\dot{\boldsymbol{V}}_{\rm E}$ and $\dot{\boldsymbol{V}}_{\rm B}$ deviate from the basic operating point. However, these voltage-related errors are not significant in this study. There are mainly two reasons. First, $\dot{\boldsymbol{V}}_{\text{E}}$ and $\dot{\boldsymbol{V}}_{\text{B}}$ are highly correlated in the ADN. For example, the increase of power output of the RES units will lead to the increase of the magnitude and phase angle of both $\dot{\boldsymbol{V}}_{\text{E}}$ and $\dot{\boldsymbol{V}}_{\text{B}}$, and vice versa. From the (11), we can observe that this correlation will offset some errors caused by the variance of voltage because $\dot{\boldsymbol{V}}_{\text{E}}$ and $\dot{\boldsymbol{V}}_{\text{B}}$ are in the numerator and the denominator part of the equation, respectively. Second, using the voltage regulation devices such as static var compensators and on-load taps, ADN can control the voltage within a certain range (for example, 0.85–1.1 p.u.) for secure and economic operation. Compared with the $\dot{\boldsymbol{S}}_{\text{E}}$ in (11), $\dot{\boldsymbol{V}}_{\text{E}}$ and $\dot{\boldsymbol{V}}_{\text{B}}$ have less impact on the equivalent boundary power injections because they have a smaller range of variation. The further empirical results are presented in Section 4.1.5, which investigates and evaluates the this kind of voltage-related error.

3.2 Probabilistic equivalence using cumulant

In this paper, a PEMM using the cumulant is proposed to simultaneously ensure the consistency of both the load flow and the probabilistic characteristics. Readers are referred to [17] for the basics of cumulants.

Let $\boldsymbol{\gamma}_{P_{\text{gE}}}^{(v)}$ and $\boldsymbol{\gamma}_{P_{\text{lE}}}^{(v)}$ be the vth cumulants of the nodal active power generation and the nodal active power load in the ADN, respectively. The definitions of $\boldsymbol{\gamma}_{Q_{\text{gE}}}^{(v)}$ and $\boldsymbol{\gamma}_{Q_{\text{lE}}}^{(v)}$ are similar. Supposing that the nodal power generation and the nodal load are independent, the vth cumulants of active power injection $\gamma_{P_{\text{E}}}^{(v)}$ and the vth cumulants of reactive power injection $\gamma_{Q_{\text{E}}}^{(v)}$ can be obtained using the additivity of cumulants:

$$\boldsymbol{\gamma}_{P_{\text{E}}}^{(v)} = \boldsymbol{\gamma}_{P_{\text{gE}}}^{(v)} + \boldsymbol{\gamma}_{P_{\text{lE}}}^{(v)}, \tag{16}$$

$$\boldsymbol{\gamma}_{Q_{\text{E}}}^{(v)} = \boldsymbol{\gamma}_{Q_{\text{gE}}}^{(v)} + \boldsymbol{\gamma}_{Q_{\text{lE}}}^{(v)}. \tag{17}$$

After we obtain $\boldsymbol{\gamma}_{P_{\text{E}}}^{(v)}$ and $\boldsymbol{\gamma}_{Q_{\text{E}}}^{(v)}$, we can deduce the expressions for the cumulants of the equivalent boundary power injections. For clarity, we first suppose that the nodal power injections in the ADN are uncorrelated. Based on (12) and (13) in Section 3.1, by means of the properties of homogeneity and the additivity of cumulants [17], the vth cumulants of the equivalent boundary power injections can be deduced as

$$\boldsymbol{\gamma}_{\Delta P_{\text{B}}}^{(v)} = \boldsymbol{E}_{\text{P}}{}^{\circ v}\boldsymbol{\gamma}_{P_{\text{E}}}^{(v)} + \boldsymbol{E}_{\text{Q}}{}^{\circ v}\boldsymbol{\gamma}_{Q_{\text{E}}}^{(v)}, \tag{18}$$

$$\boldsymbol{\gamma}_{\Delta Q_{\text{B}}}^{(v)} = -\boldsymbol{E}_{\text{Q}}{}^{\circ v}\boldsymbol{\gamma}_{P_{\text{E}}}^{(v)} + \boldsymbol{E}_{\text{P}}{}^{\circ v}\boldsymbol{\gamma}_{Q_{\text{E}}}^{(v)}, \tag{19}$$

where $[\,*\,]^{\circ v}$ is the Hadamard power operator.

Note that the derivation presented above takes the advantage of the additivity and homogeneity of the cumulant and the additivity under the condition that the stochastic variables are independent.

PEMM based on (18) and (19) has the following characteristics: (i) the application of cumulant avoids the complicated convolution operation between random variables and greatly simplifies the work of equivalence; (ii) (18) and (19) are presented in a PQ decoupling manner, which makes the incorporation of the active and reactive power injections in ADN flexible and independent; (iii) the derivation of the PEMM utilised the information of the network topology and power loss of ADN. Hence, it can consider the heterogeneity of the nodal power injections in the ADN instead of treating them without distinction, which improves the accuracy of the equivalent model and (iv) PEMM only relies on the operation information of ADNs.

$\boldsymbol{\gamma}_{\Delta P_{\text{B}}}^{(v)}$ and $\boldsymbol{\gamma}_{\Delta Q_{\text{B}}}^{(v)}$ aggregate the uncertainty of power loss and power injections in ADNs, which contain the probabilistic information of ADNs. The moments of the equivalent boundary power injections can be obtained using the relationship between cumulant and moment [17], which can facilitate further analysis of transmission networks by avoiding the complication of ADN models. Compared with the original CTDS, the equivalent network obtained from the PEMM is less complicated but still preserves the consistency of the probabilistic characteristics and the consistency of the load flow.

3.3 Consideration of correlations

The PEMM derived in Section 3.2 does not consider the correlations of RESs in the ADN. This section uses an orthogonal transformation to incorporate the correlations into the PEMM [18]. For convenience, we focus on discussing the correlations of active power generation.

Let $\boldsymbol{P}$ be the correlated active power injection vector in the ADN:

$$\boldsymbol{P} = (p_1, p_2, \ldots, p_m), \tag{20}$$

with the correlation coefficient matrix $\boldsymbol{C}_{\text{p}}$.

$\boldsymbol{C}_{\text{p}}$ is usually symmetric and also positive definite. Thus, Cholesky decomposition can be used to decompose $\boldsymbol{C}_{\text{p}}$ [18]:

$$\boldsymbol{C}_{\text{p}} = \boldsymbol{G}\boldsymbol{G}^{\text{T}}. \tag{21}$$

Then, the correlated active power injection $\boldsymbol{P}$ can be transformed into uncorrelated random variable $\boldsymbol{P}'$:

$$\boldsymbol{P}' = \boldsymbol{G}^{-1}\boldsymbol{P}. \tag{22}$$

Conversely, the corresponding inverse orthogonal transformation can be expressed as

$$\boldsymbol{P} = \boldsymbol{G}\boldsymbol{P}'. \tag{23}$$

As formulated in (23), we can express the correlated vth cumulants of the nodal active power injection in the ADN as the weighted linear combination of independent vth cumulants using the inverse orthogonal transformation:

$$\gamma_{P_{\text{E},j}}^{(v)} = \sum_{r=1}^{j} g_{jr}^{v}\gamma_{P'_{\text{E},j}}^{(v)},\ j = 1, 2, \ldots, m, \tag{24}$$

where $\gamma_{P'_{\text{E},j}}^{(v)}$ is the uncorrelated cumulant of active power injection in bus j of the ADN, m is the number of buses of the ADN, and g_{jr}^{v} is the jth row and rth column element of the matrix $\boldsymbol{G}^{v}$.

By performing an orthogonal transformation, the correlated active power injections $\boldsymbol{P}$ can be transformed into uncorrelated random variables. Then, substituting (24) into (18) and (19) yields

$$\gamma_{\Delta P_{\text{B}}}^{(v)} = \tilde{\boldsymbol{E}}_{\text{P}}{}^{\circ v}\gamma_{P'_{\text{E}}}^{(v)} + \boldsymbol{E}_{\text{Q}}{}^{\circ v}\gamma_{Q_{\text{E}}}^{(v)}, \tag{25}$$

$$\gamma_{\Delta Q_{\text{B}}}^{(v)} = -\tilde{\boldsymbol{E}}_{\text{Q}}{}^{\circ v}\gamma_{P'_{\text{E}}}^{(v)} + \boldsymbol{E}_{\text{P}}{}^{\circ v}\gamma_{Q_{\text{E}}}^{(v)}. \tag{26}$$

The elements of $\tilde{\boldsymbol{E}}_{\text{P}}{}^{\circ v}$ and $\tilde{\boldsymbol{E}}_{\text{Q}}{}^{\circ v}$ can be calculated by

$$\tilde{e}_{\text{p},ir}^{v} = \sum_{k=r}^{m} e_{\text{p},ik}^{v}\, g_{kr}^{v},\ r = 1, 2, \ldots, m, \tag{27}$$

$$\tilde{e}_{\text{q},ir}^{v} = \sum_{k=r}^{m} e_{\text{q},ik}^{v}\, g_{kr}^{v},\ r = 1, 2, \ldots, m, \tag{28}$$

where $e_{\text{p},ik}^{v}$ is the element of $\boldsymbol{E}_{\text{P}}^{\circ v}$ in the ith row and kth column, $e_{\text{q},ik}^{v}$ is the element of $\boldsymbol{E}_{\text{Q}}^{\circ v}$ in the ith row and kth column, i is the index of the boundary buses and r is the index of the buses of the ADN.

With (25) and (26), the PEMM can consider the correlations among the active power injections in the ADN. A similar

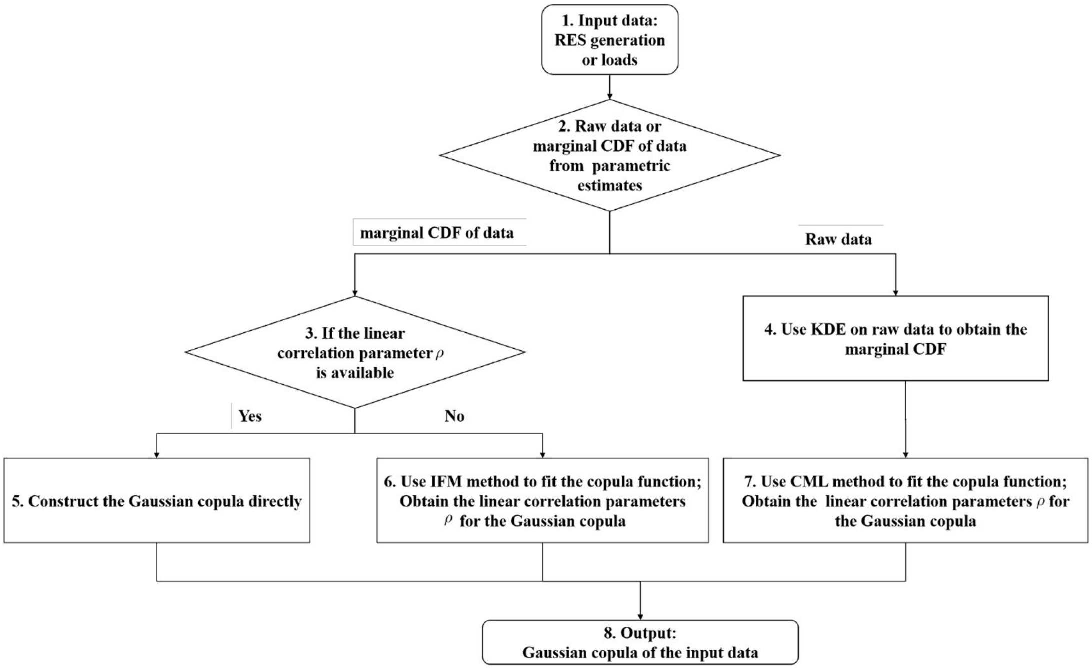

Fig. 3 *Flowchart of the derivation of the copula function*

procedure can be used to consider correlated reactive power injections.

3.4 The joint cumulant of the power injection in ADNs

When applying the PEMM for ADNs, the first step is to obtain the cumulants of the power injections in the ADN. In the case that multiple PV plants or WFs are integrated into an ADN, the probabilistic model for renewable power generation is actually a multivariate distribution. When the outputs of WFs and PV plants are correlated, the $\gamma^{(v)}_{P_{\text{pv, E}}}$, $\gamma^{(v)}_{P_{\text{wind, E}}}$, $\gamma^{(v)}_{Q_{\text{pv, E}}}$ and $\gamma^{(v)}_{Q_{\text{wind, E}}}$ are supposed to be joint cumulants. However, it is intractable to obtain the joint probability distribution function for this multivariate distribution, and therefore, it is difficult to obtain the joint cumulants directly [12].

In this section, we develop a sampling-based method to obtain the joint cumulants for the correlated power injections, which utilises the copula function to describe the correlation structures.

The copula function can connect multiple univariate distributions to a multivariate distribution [19]. With marginal probability distributions for each random power injection and the correlation information, such as the Pearson correlation coefficient ρ, the copula function can be used to connect these dispersive marginal probability distributions and to generate the samples of the correlated random variables.

The Sklar theorem states that any multivariate joint distribution $F(x_1, x_2, \ldots, x_N)$ can be expressed by the combination of N univariate marginal cumulative distribution functions (CDFs) $F_1(x_1), F_2(x_2), \ldots, F_N(x_N)$ and a copula function $C(u_1, u_2, \ldots, u_N)$ defined in the N-dimensional space $[0, 1]^N$:

$$F(x_1, x_2, \ldots, x_N) = C(F_1(x_1), F_2(x_2), \ldots, F_N(x_N)) . \tag{29}$$

The Gaussian copula function is used to obtain the correlated samples of power generation and loads in the ADN. The CDF of the Gaussian copula function can be expressed as

$$C(u_1, u_2, \ldots, u_N; \boldsymbol{\rho}) = \varphi_{\boldsymbol{\rho}}(\varphi^{-1}(u_1), \varphi^{-1}(u_2), \ldots, \varphi^{-1}(u_N)), \tag{30}$$

where $\boldsymbol{\rho}$ is the correlation coefficient matrix; $\varphi_{\boldsymbol{\rho}}$ is the CDF of the standard multivariate Gaussian distribution with correlation coefficient matrix $\boldsymbol{\rho}$ and φ^{-1} is the inverse CDF of standard univariate Gaussian distribution.

It is noted that this paper aims to develop the equivalent method for ADN, in which the correlated random power injections are considered. The proposed method is not limited to a specific distribution type, and it can be applied to the raw RES and load samples as well. Fig. 3 presents the flowchart of the derivation of the Gaussian copula function of the data. The details are given below.

1. Input the data of RES or load. It could be the raw data samples or the marginal CDFs of data from the parametric estimates.
2. If the input data is the raw dataset, go to step 4 and if the input data is the marginal CDF, go to step 3.
3. If the linear correlation parameter among the different RESs or the different loads is available, go to step 5; otherwise go to step 6.
4. Use the non-parametric techniques such as kernel density estimation (KDE) on raw data to obtain the marginal CDF of the data.
5. Construct the Gaussian copula directly.
6. Use inference functions for margins [20] to fit the copula function and Obtain the linear correlation parameter for the Gaussian copula.
7. Use canonical maximum likelihood [21] to fit the copula function and obtain the linear correlation parameter for the Gaussian copula.
8. Output the Gaussian copula φ_ρ of the input data and the marginal CDFs of input data.

After obtaining the marginal CDF of the data and their corresponding copula functions, the steps in obtaining the joint cumulants of the power injections are as follows:

(i) Obtain the CDF of the Gaussian copula function φ_ρ.
(ii) Using the Gibbs sampling technique [22], obtain the samples of the Gaussian copula distribution $\boldsymbol{C}_{N \times M} = [\boldsymbol{c}_1, \boldsymbol{c}_2, \ldots, \boldsymbol{c}_M]$, where N is the number of samples and M is the dimension of the variable.
(iii) Obtain the correlated wind speed or solar irradiation samples $\boldsymbol{Z}_{N \times M} = [z_1, z_2, \ldots, z_M]$ with the $\boldsymbol{C}_{N \times M}$ and the marginal CDF of wind speed or solar irradiation F_j, as illustrated in Fig. 4

$$z_i = F_i^{-1}(\boldsymbol{c}_i), \quad i = 1, 2, \ldots, M . \tag{31}$$

Obtain the correlated load samples using the inverse transform sampling as well.

(iv) Obtain the correlated renewable power generation samples $\boldsymbol{x}_{\cdot i} = [x_{1i}, x_{2i}, \dots, x_{Ni}]^{\mathrm{T}}$ using (2) and (5).

(v) Obtain the joint moments of the renewable power generation and loads based on the correlated samples $\boldsymbol{x}_{\cdot i} = [x_{1i}, x_{2i}, \dots, x_{Ni}]^{\mathrm{T}}$:

$$a_{v, x_i} = \sum_{j=1}^{N} (x_{ji})^{v} / N, v = 1, 2, \dots . \tag{32}$$

(vi) Calculate the joint cumulants of the renewable power generations and loads using the relationship between moments and cumulants [17].

3.5 Flowchart

Fig. 5 gives a flowchart of the PEMM for establishing the probabilistic equivalent model of the ADN. The proposed equivalent method only needs the system data of the distribution systems, which means that it can be developed by the DSOs independently. This characteristic gets rid of the need for the DSOs to share their detailed models and operation information with the TSOs, thereby protecting the commercially sensitive information of DSOs. Thus, the proposed method is useful for integrated transmission and distribution analysis. As a coordination tool for DSOs and TSOs, the proposed method can improve the reliability and efficiency of the transmission systems by enabling the TSOs to take the uncertainty of the loads and renewable generation in the distribution system into account in an accurate way.

4 Case studies

To illustrate the validity of the proposed probabilistic equivalent method, two test systems on different scales are considered. One of the systems consists of a 14-bus transmission system and a 33-bus radial distribution system, and the other is a larger scale power grid, which is composed of a 118-bus transmission system and three radial distribution systems of different scale. The effectiveness of the probabilistic equivalent method is demonstrated by comparison with the original model in terms of efficiency and accuracy.

All tests are performed on a computer with Core i5 processor running at 2.6 GHz and 8 GB of RAM. The code is implemented on the platform of MATLAB R2019b.

4.1 Case I: CTDS of a 14-bus transmission system and a 33-bus radial distribution system

In Case I, the system configuration is detailed in Section 4.1.1. The relevant PLF calculation embedded with PEMM is introduced in Section 4.1.2. Section 4.1.3 investigates and evaluates the accuracy of the probabilistic equivalent model obtained from PEMM through the comparison with the LR method. Section 4.1.4 discusses the impact of the reactive power output of RES units on the equivalent model. The computational efficiency by using the probabilistic equivalent model is presented in Section 4.1.5.

4.1.1 System configuration: To demonstrate the effectiveness of the proposed method, case studies are performed on a CTDS system. The transmission side of this CTDS is the modified IEEE 14-bus system shown in Fig. 6 and the parameters of the system are detailed in [23]. The distribution side of the CTDS is based on the modified IEEE 33-bus system shown in Fig. 7, and the parameters of the system are detailed in [23]. The voltage base of the distribution network is 12.66 kV. The ADN is connected to the transmission system through bus 13 in the transmission system, which is regarded as the boundary bus. The reactance of the distribution transformers is 0.05 p.u. on the base of 100 MVA.

The ADN incorporates six WFs and four PV plants, and they are located on buses 6, 12, 20, 24 and 29, respectively, as shown in Fig. 7. The v_{ci}, v_{co} and v_{N} of the wind turbines in these six WFs are 3, 14 and 25 m/s, respectively. The power factor of the WFs and PV plants are set to 1 for simplicity. It should be pointed out that the setting of this power factor does not affect the applicability of the method in this paper and the relevant discussion is presented in

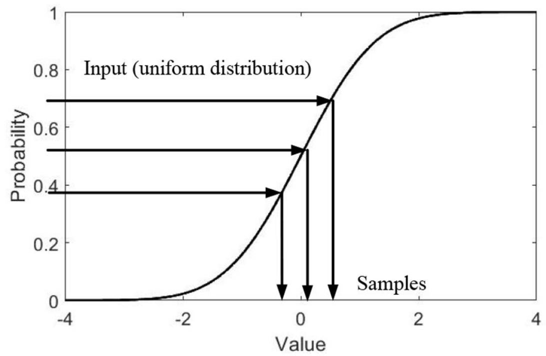

Fig. 4 *Example of inverse transform sampling*

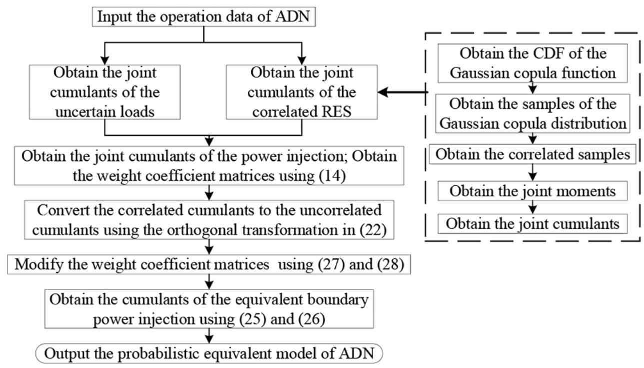

Fig. 5 *PEMM for ADNs*

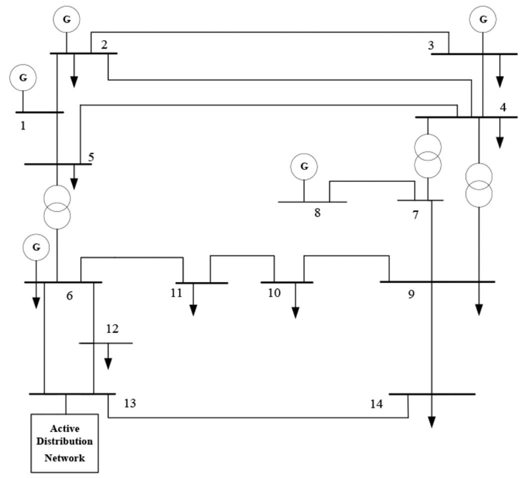

Fig. 6 *Modified IEEE 14-bus power system with integrated ADN*

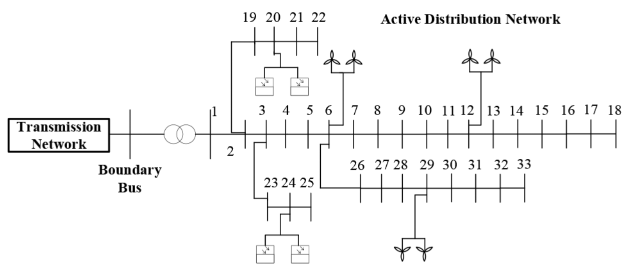

Fig. 7 *Modified IEEE 33-bus distribution network*

Section 4.1.4. The scale parameter and the shape parameter of the wind speed distribution are set to 2.8 and 5.14, respectively. Concerning PV plants, the parameters of the distribution of the active power output are 3.3 and 3.1. In this case, the penetration level of the RES is 11.15%. To emphasise the impact of the uncertainty of RES and loads in the ADN on the transmission grid, no RES plants are involved in the transmission grid, which means

Table 1 Cumulants of the equivalent boundary power injections at bus 13

	$\gamma^{1}_{P\text{eq}}$	$\gamma^{2}_{P\text{eq}}$	$\gamma^{3}_{P\text{eq}}$	$\gamma^{4}_{P\text{eq}}$
PEMM	3.47×10^{-2}	1.79×10^{-6}	-2.78×10^{-11}	-3.15×10^{-13}
LR	3.47×10^{-2}	0.78×10^{-6}	0.65×10^{-11}	0.28×10^{-13}
	$\gamma^{1}_{Q\text{eq}}$	$\gamma^{2}_{Q\text{eq}}$	$\gamma^{3}_{Q\text{eq}}$	$\gamma^{4}_{Q\text{eq}}$
PEMM	2.42×10^{-2}	5.86×10^{-7}	-4.41×10^{-21}	-3.29×10^{-26}
LR	2.42×10^{-2}	4.54×10^{-7}	-1.08×10^{-11}	1.39×10^{-14}

that the only uncertain sources in the transmission grid are from the ADNs.

The correlation between wind speeds among the six WFs is considered, as is the correlation between solar irradiances among the four PV plants. The correlation coefficients for the wind speeds or solar irradiances within the same node are relatively high. The correlation coefficient matrices for the wind speeds in the WFs and the solar irradiances at the four PV plants are as follows:

$$\boldsymbol{\rho}_{\text{wind}}=\begin{bmatrix}1&0.9&0.6&0.6&0.4&0.4\\0.9&1&0.6&0.6&0.4&0.4\\0.6&0.6&1&0.9&0.5&0.5\\0.6&0.6&0.9&1&0.5&0.5\\0.4&0.4&0.5&0.5&1&0.9\\0.4&0.4&0.5&0.5&0.9&1\end{bmatrix},$$

$$\boldsymbol{\rho}_{\text{PV}}=\begin{bmatrix}1&0.9&0.5&0.5\\0.9&1&0.5&0.5\\0.5&0.5&1&0.9\\0.5&0.5&0.9&1\end{bmatrix}.$$

In this case, for the uncertain loads in the ADN, their expected values are set to their deterministic value and the standard deviations are set to 10% of the expected values. For simplicity, the correlation between loads of different buses is not considered in this case. Because the normal distribution is used to describe the uncertainty of the loads, their cumulants can be calculated as follows:

$$\gamma^{(1)}_{\text{load}}=\mu,\gamma^{(2)}_{\text{load}}=\sigma^2,\gamma^{(v)}_{\text{load}}=0,\quad \text{for}\quad v\ge 3 \tag{33}$$

4.1.2 PLF calculation embedded with PEMM: PLF is an essential tool for analysing the uncertain states of power systems. The equivalent models derived from PEMM are supposed to be integrated into the PLF algorithms to alleviate the computational burden of these algorithms. The coordination between the PEMM and the two types of well-known PLF algorithms, and the cumulant-based PLF (CPLF) and Monte Carlo simulation-based PLF (MCS-PLF), are discussed. The performance of the proposed PEMM will be evaluated using CPLF and MCS-PLF in the following section.

With the cumulants of the equivalent boundary power injections obtained from the PEMM, the probabilistic equivalent model can be readily integrated into the CPLF [24].

The equivalent boundary power injections can be regarded as an equivalent generator representing the ADN. Then, CPLF can be performed on the probabilistic equivalent model. The procedure is detailed as follows [24]:

(i) Obtain the cumulants of the equivalent boundary power injections using the PEMM.
(ii) Compute the cumulants of the power injections of other buses except for the boundary bus according to the given probabilistic distribution.
(iii) Compute the cumulants of the state variables, including the voltage and branch flow according to the cumulants of the power injections and the linearised power flow equation.
(iv) Construct the CDF and PDF of the state variables using Gram–Charlier expansion [24], maximum entropy method [25] or another method.

MCS-PLF relies on the samples of variables and the deterministic load flow. The procedure for MCS-PLF using the probabilistic equivalent model is developed as follows:

(i) Compute the cumulants of the equivalent boundary power injection using the PEMM.
(ii) Calculate the Gram–Charlier expansion coefficients of the equivalent boundary power injection using the corresponding cumulants and then obtain the CDF of the equivalent boundary power injection F_{eq}.
(iii) Generate samples from the uniform distribution $U_M=[u_1,u_2,\ldots,u_M]$ and obtain samples of the equivalent boundary power injection using the inverse CDF: $e_i=F^{-(1}_{\text{eq}}(u_i)\quad i=1,2,\ldots,M$ as shown in Fig. 4.
(iv) Run the deterministic load flow based on the samples of the equivalent boundary power injection.
(v) Obtain the statistics of the state variables according to the results of the deterministic load flow.

4.1.3 Evaluation of PEMM: To evaluate the performance of the proposed PEMM, an alternative equivalent modelling method, called the LR method, is presented. The basic idea of the LR is to construct the equivalent boundary power injection by simply aggregating the RES generations, the loads and the power loss in the ADNs with an estimated LR. This method is based on the sample set of the ADN, where each sample contains the data for the RES generations and the loads. The LR is an intuitively straightforward way to construct the equivalent model for the distribution network and it is one kind of PQ equivalence [26]. This paper conducts a series of comparative experiments to validate the proposed PEMM in comparison with LR. The detailed process of the LR is as follows:

(i) Obtain the nodal power injections $P_{\text{inj},0}$ and $Q_{\text{inj},0}$, the active power loss $P_{\text{loss},0}$ and the reactive power loss $Q_{\text{loss},0}$ in the ADN under the basic operating point, which is derived from the expected values of the sample set.
(ii) Compute the active and reactive power LRs, respectively

$$\Phi_{\text{P}}=\frac{P_{\text{loss},0}}{P_{\text{inj},0}},\Phi_{\text{Q}}=\frac{Q_{\text{loss},0}}{Q_{\text{inj},0}}. \tag{34}$$

(iii) For the ith sample in the sample set, compute the equivalent boundary power injections:

$$P_{\text{eq},i}=P_{\text{inj},i}*(1+\Phi_{\text{P}}),Q_{\text{eq},i}=Q_{\text{inj},i}*(1+\Phi_{\text{Q}}), \tag{35}$$

(iv) Compute the moments of the equivalent boundary power injections based on the sample set.
(v) Compute the cumulants using the relationship between the moments and the cumulants and obtain the probabilistic model of the equivalent boundary power injections.

Applying the PEMM and LR to the test system, probabilistic equivalent models with the uncertain boundary power injection at bus 13 can be obtained and their cumulants are presented in Table 1. Moreover, for PEMM, since few shunt components exist in this ADN, the equivalent shunt conductance and shunt susceptance at bus 13 are -3.55×10^{-13} and 3.55×10^{-13} p.u., respectively, which can be derived from $\boldsymbol{Y}_{\text{BB}}-\boldsymbol{Y}_{\text{BE}}\boldsymbol{Y}^{-1}_{\text{EE}}\boldsymbol{Y}_{\text{EB}}$ in (10).

To evaluate the accuracy of the obtained probabilistic equivalent model, PLFs are performed on the original and the equivalent models, respectively. The results of the MCS-PLF of the original system are regarded as the benchmarks and the number of MCS is set to 5000 in this case.

Figs. 8–10 show the PDF curves of selected state variables, which are derived from different PLF algorithms and models. The legends of these figures are summarised in Table 2. Notably, the branches in Figs. 8 and 9 are directly connected to the boundary

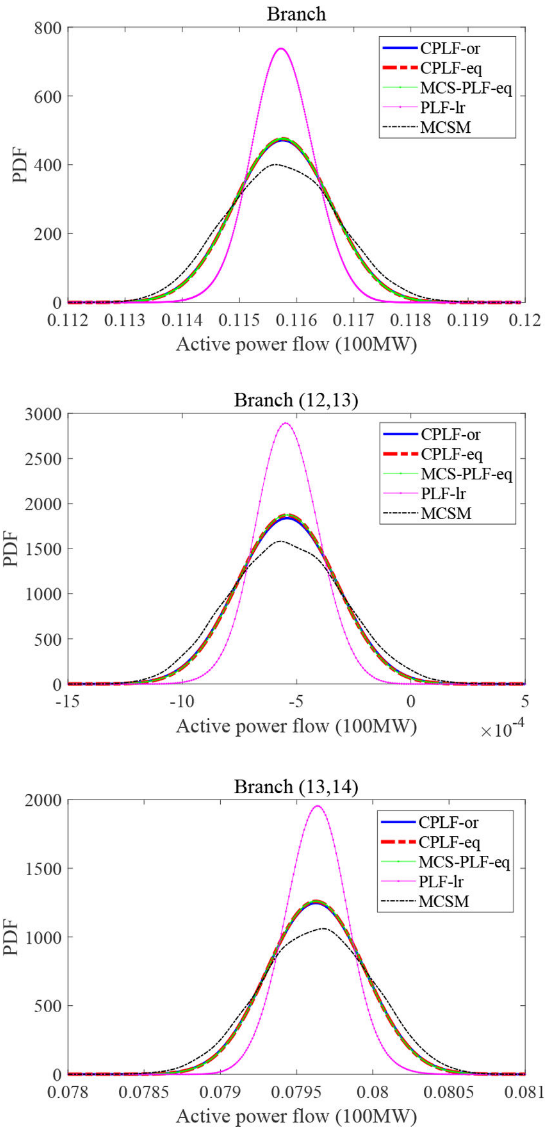

Fig. 8 *PDF curves of the active power flow of the branches connected to boundary buses in IEEE 14-bus system*

Table 2 Legend in figures

Legend	PLF algorithms	Model
MCSM	MCS-PLF	original model
CPLF-or	CPLF	original model
PLF-lr	CPLF	equivalent model from LR
CPLF-eq	CPLF	equivalent model from PEMM
MCS-PLF-eq	MCS-PLF	equivalent model from PEMM

bus 13, which means that they are more likely to be affected by the accuracy of the equivalent model.

Compared with the PLF-lr curves, the CPLF-eq and MCS-PLF-eq curves are close to the MCSM curves. The equivalent models derived from PEMM are superior to those derived from LR in terms of accuracy. Both the result of MCSM and CPLF-or are based on the original model. The gap between MCSM and CPLF-or demonstrates there are errors in the result of CPLF because of the assumption and approximation made in the CPLF algorithm. The only difference between the CPLF-or and the CPLF-eq is the model. Hence, the similar results of the CPLF-or and the CPLF-eq demonstrate the equivalent model derived from PEMM is pretty accurate in the context of the CPLF algorithm. The difference between the MCS-PLF-eq and the MCSM indicates that the performance of the equivalent model in the context of MCS-PLF is not as good as that in the context of CPLF. The reason is that the derivation of PEMM is based on the property of the cumulant,

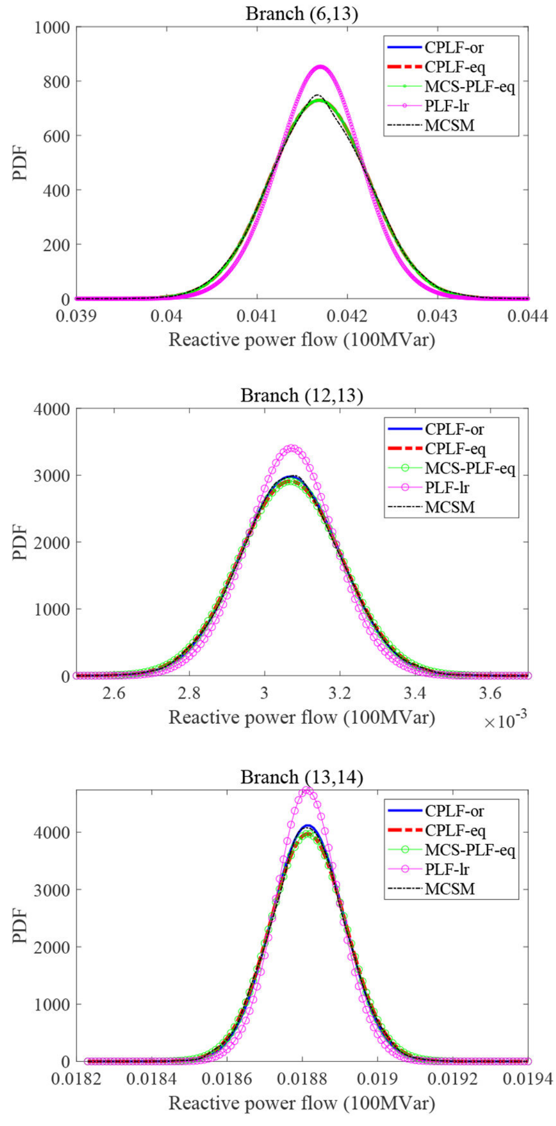

Fig. 9 *PDF curves of the reactive power flow of the branches connected to boundary buses in IEEE 14-bus system*

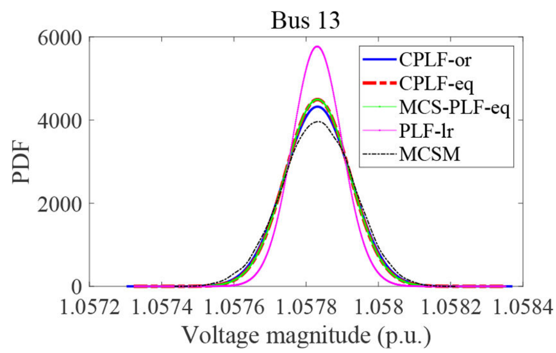

Fig. 10 *PDF curves of the voltage magnitude of bus 13*

which relies on some assumptions and simplification. Even so, the curves of the equivalent model, such as CPLF-eq and MCS-PLF-eq, are still close to the curves of the MCSM, which can substantiate the effectiveness of the proposed PEMM.

Fig. 11 shows the average root mean square (ARMS) errors of all active power flows, reactive power flows and PQ bus voltage magnitudes of the transmission system using the CDF of the MCSM results as a reference. The ARMS error is defined as

$$\mathrm{ARMS} = \frac{\sqrt{\sum_{i=1}^{N} (C_{t,i} - C_{\mathrm{MCSM},i})}}{N}, \tag{36}$$

where $C_{\mathrm{MCSM},i}$ is the ith value of the CDF of the MCSM result, $C_{t,i}$ is the corresponding ith value of the CDF of the other results, t is the index for the other results and N is the number of points. In this case, N is set to 10,000. Notably, the 14th branch (branch (7,8) in the 14-bus system) in Fig. 11 is not presented because there is no active power flow on this branch. These figures show that the equivalent model obtained from the PEMM is more accurate than that obtained from the LR. For example, the average ARMS error of CPLF-eq of active power flow is 0.0012, which is smaller than that of PLF-lr by 69.23%. The maximum ARMS error of CPLF-eq of active power flow is 0.0042, which is smaller than that of PLF-lr by 64.71%. The minor gaps between the CPLF-or curves and the CPLF-eq curves confirm that the equivalent model can depict the probabilistic characteristics of the ADN relatively well.

The LR method aggregates all the power injections in ADNs first and builds the equivalent model using two constant power LRs only. By contrast, the PEMM transfer the uncertainty of the RES and loads to the boundary considering the network topology and parameters of the ADN. The PEMM considers the heterogeneity of the nodal power injections in the ADN instead of treating them without distinction. Hence, the probabilistic equivalent models obtained from the PEMM are more accurate. Moreover, as shown in Fig. 12, the power LRs vary in a wide range in the ADN because the penetration of large-scale renewables makes the directions of power flow complicated. This characteristic is also a reason for the deterioration of the accuracy of the LR method.

4.1.4 Impact of the reactive power output of RES: To evaluate the influences of the reactive power output of the renewable energy (RE) units upon the equivalent model, three probabilistic equivalent models based on the test system of Case I under three scenarios are constructed. In these three scenarios, the power factor of RE units is set as 0.98 (lagging), 0.98 (leading) and 1.00, respectively. The lagging scenario represents that the RE units consume reactive power, while the leading scenario represents that the RE units generate reactive power. The cumulants of the equivalent boundary power injections at the boundary bus of these three scenarios are listed in Table 3. The reactive power output of the RES units has few influences on the equivalent boundary active power injections. However, the reactive power output of the RE units leads to the variation of the equivalent boundary reactive power injections. First, from the data of the first-order cumulants, the lagging power factor will increase the reactive power consumption in the distribution system, whereas the leading power factor will decrease the reactive power consumption. Second, from the data of the second-order cumulants, both the lagging power factor and leading power factor lead to the higher variance of the equivalent boundary reactive power injections compared with the unit power factor. This is because the reactive power of RES units is stochastic and the involvement of these stochastic variables will increase the uncertain degree of the reactive power part of the probabilistic equivalent models. The similar findings can be observed in the higher-order cumulants. With the higher variance of the equivalent boundary reactive power injections, it is expected that the voltage magnitude and reactive power branch flow of the transmission system will fluctuate in a larger range.

4.1.5 Analysis of voltage-related error: PEMM developed in (12) and (13) utilises the $\dot{\boldsymbol{V}}_{\mathrm{E}}$ and $\dot{\boldsymbol{V}}_{\mathrm{B}}$ at basic operating point to derive $\boldsymbol{E}_{\mathrm{P}}$ and $\boldsymbol{E}_{\mathrm{Q}}$, which are the decoupled power transfer matrices. This section investigates and appraises the voltage-related error discussed in Section 3.1.

In this case study, we assume the voltage error is caused by the variable consumption of the stochastic loads in the ADN. There are two reasons for this setting. One is that the sum of the expected consumption of the loads outweighs the output of the RES in our case. Hence, the fluctuation of voltage caused by the loads is more significant. The other reason is that in Case I, the loads are assumed to follow the normal distribution, for which it is easier to quantify the dispersion of the random variables. It is noted that the findings and comments derived from this case study can be generalised to the voltage errors caused by the RES as long as the total output of the RES does not exceed the amounts of the loads.

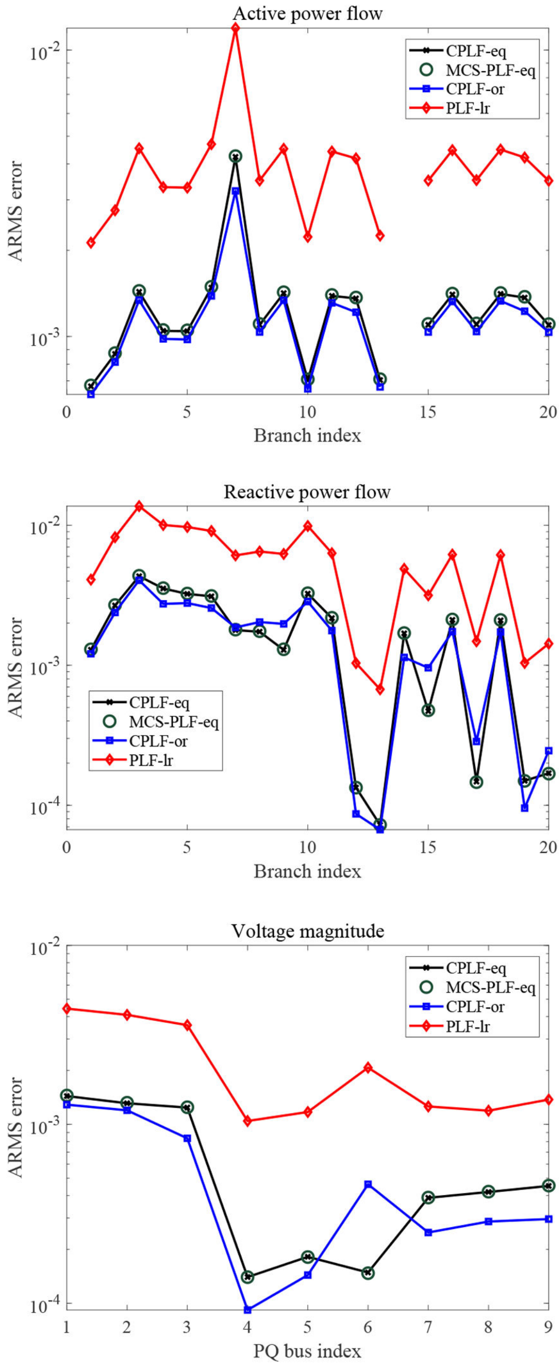

Fig. 11 *ARMS errors of active power flow, reactive power flow and voltage magnitude in the IEEE 14-bus system*

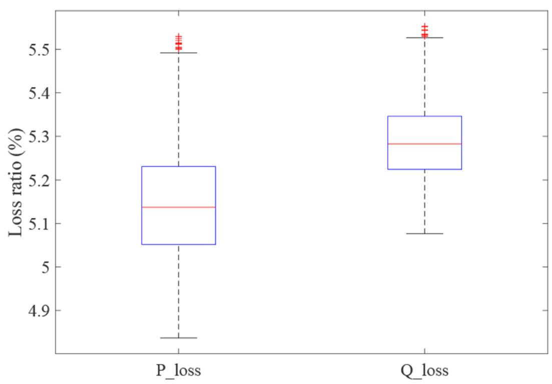

Fig. 12 *Box plot of the power LR of the ADN in Case I*

Four equivalent models are developed using four sets of $\dot{V}_E$ and $\dot{V}_B$ at different operating points. The first model, denoted as M1, is derived at the basic operating point, in which the actual consumption of the loads is exactly their expected value. The second model, denoted as M2, is derived at the random operating point, in which the actual consumption of the loads is generated by randomly sampling from their distributions. The other two models, denoted as M3 and M4, respectively, are derived at the deviated operating points, in which the actual consumption of the loads is assumed to be one standard deviation higher or lower than the expected value, respectively. The scenarios of M3 and M4 are relatively extreme because all the loads deviate in the same direction concurrently and thus no up/down offsets exist. The main differences among these four models are the value of the power transfer matrices $\boldsymbol{E}_P$ and $\boldsymbol{E}_Q$.

Table 4 shows the probabilistic information of these four equivalent models. Even though the value of $\dot{V}_E$ and $\dot{V}_B$ will impact the equivalent models, the magnitude of such impacts is insignificant. To be specific, $\gamma^2_{P\mathrm{eq}}$ and $\gamma^2_{Q\mathrm{eq}}$, which can also be interpreted as the variance of the equivalent boundary bus power injections, of these four models are extremely close. Besides, the higher-order cumulants, e.g. $\gamma^3_{P\mathrm{eq}}$ and $\gamma^4_{P\mathrm{eq}}$, of these four models are in good agreement with each other. In terms of $\gamma^3_{Q\mathrm{eq}}$ and $\gamma^4_{Q\mathrm{eq}}$, though the discrepancy exists, the impact of this discrepancy on the performance of the equivalent models is negligible because their orders of magnitude lie in the range of $[10^{-20}, 10^{-22}]$ and $[10^{-25}, 10^{-27}]$, which is relatively tiny compared to the orders of magnitude of $\gamma^2_{Q\mathrm{eq}}$. Thus, the proposed PEMM is robust to the voltage-related errors we discuss in Section 3.1 based on the empirical results.

To account for the satisfactory performance of PEMM on the voltage-related errors, we calculate the magnitude and phase angle of $\dot{V}_B$ and $\dot{V}_E$. Considering that $\dot{V}_B$ has one element and $\dot{V}_E$ has 33 elements in Case I, we compare the $\dot{V}_B$ to the average of $\dot{V}_E$, which is listed in Table 5, where $\boldsymbol{\theta}_B/\boldsymbol{\theta}_E^{\mathrm{ave}}$ and $|\boldsymbol{V}_B|/|\boldsymbol{V}_E^{\mathrm{ave}}|$ are the ratio of the voltage phase angle and voltage magnitude of boundary bus to the average voltage phase angle and magnitude of external bus, respectively. It is shown that the ratios of the voltage of boundary bus to external buses is quite similar, which indicates the positive correlation between $\dot{V}_E$ and $\dot{V}_B$. This correlation will offset some voltage-related errors caused by the variance of voltage because $\dot{V}_E$ and $\dot{V}_B$ are in the numerator and the denominator part of (11), respectively. That is a vital reason for the satisfactory performance of PEMM on the voltage-related errors.

Table 3 Cumulants under different power factors

Power factor	$\gamma^1_{P\mathrm{eq}}$ / 10^{-2}	$\gamma^2_{P\mathrm{eq}}$ / 10^{-6}	$\gamma^3_{P\mathrm{eq}}$ / 10^{-11}	$\gamma^4_{P\mathrm{eq}}$ / 10^{-13}
0.98 (lagging)	−3.47	1.79	−2.78	−3.16
0.98 (leading)	−3.47	1.79	−2.78	−3.15
1.00	−3.47	1.79	−2.78	−3.15
power factor	$\gamma^1_{Q\mathrm{eq}}$ / 10^{-2}	$\gamma^2_{Q\mathrm{eq}}$ / 10^{-7}	$\gamma^3_{Q\mathrm{eq}}$ /10^{-13}	$\gamma^4_{Q\mathrm{eq}}$ / 10^{-16}
0.98 (lagging)	−2.51	6.29	2.33	−5.37
0.98 (leading)	−2.34	6.28	−2.32	−5.35
1.00	−2.42	5.86	-4.41×10^{-8}	-3.29×10^{-10}

Table 4 Equivalent models under different operating points

Model	$\gamma^2_{P\mathrm{eq}}$ / 10^{-6}	$\gamma^3_{P\mathrm{eq}}$ / 10^{-11}	$\gamma^4_{P\mathrm{eq}}$ / 10^{-13}
M1	1.79	−2.78	−3.15
M2	1.79	−2.79	−3.16
M3	1.80	−2.80	−3.18
M4	1.78	−2.77	−3.13
Model	$\gamma^2_{Q\mathrm{eq}}$ / 10^{-7}	$\gamma^3_{Q\mathrm{eq}}$ / 10^{-13}	$\gamma^4_{Q\mathrm{eq}}$ / 10^{-16}
M1	5.86	-4.41×10^{-8}	-3.29×10^{-10}
M2	5.87	-8.01×10^{-8}	-8.19×10^{-10}
M3	5.95	-1.34×10^{-7}	-1.39×10^{-9}
M4	5.78	-8.21×10^{-9}	-3.75×10^{-11}

Table 5 Ratios of the voltage of boundary bus to external buses

	$\boldsymbol{\theta}_B/\boldsymbol{\theta}_E^{\mathrm{ave}}$	$\lvert\boldsymbol{V}_B\rvert/\lvert\boldsymbol{V}_E^{\mathrm{ave}}\rvert$
M1	0.9958	1.048
M2	0.995	1.0536
M3	0.9966	1.0425
M4	0.9960	1.0478

Table 6 Computational efficiency of different models in Case I

	t_m, s	t_c, s	n_{var}
MCSM	-	22.843	194
CPLF-or	-	0.392	194
PLF-lr	0.160	0.016	62
CPLF-eq	**0.054**	**0.017**	62
MCS-PLF-eq	**0.054**	**13.321**	62

4.1.6 Computational efficiency: The computational efficiency of the algorithms in Section 4.1.3 is presented in Table 6, where t_m is the time consumed in the equivalent modelling, t_c is the time consumed in the PLF calculation and n_{var} is the number of unknown state variables in the system. The data in Table 6 is obtained by averaging ten independent runs. Herein the unknown state variables include the voltage magnitude and phase angle of PQ nodes, the phase angle of PV nodes, and the active and reactive power flow of all branches in the transmission system. The number of Monte Carlo simulation is set to 5000 in this case.

As for the equivalent modelling, the PEMM consumes 0.054 s, which is faster than the LR method by 66.25%. Thus, the PEMM is computationally efficient for PLF. In terms of using the equivalent model to perform the PLF algorithms on the transmission system, it can save about 81.89% of the time for the CPLF calculation and about 41.45% of the time for the MCS-PLF calculation. The improvement in the efficiency is partly because n_{var} in the equivalent model is less than that in the original model by 68.04%.

It is worth mentioning that the PEMM only needs the operating data of the distribution network, so it can be completed independently by the DSOs. In practical applications, to facilitate the secure and economic operation of the transmission system, the DSOs only need to share the equivalent model of the system to the TSOs, rather than the detailed original model. Based on the results of the evaluation of the accuracy of PEMM and the computational efficiency, using the PEMM, the efficiency of the probabilistic analysis toward the transmission network can be substantially enhanced without compromising accuracy. Hence, in the context of considering the uncertain RES integrated into the ADN, the PEMM can play an important role in the coordination of the TSOs and DSOs while enabling the independent operation of the distribution network.

4.2 Case II: CTDS of a 118-bus transmission system and three radial distribution systems

To further investigate the performance of the proposed PEMM, a larger CTDS is simulated in this experiment. The system configuration is detailed in Section 4.2.1. The accuracy of the equivalent model is evaluated in Section 4.2.2. Section 4.2.3 shows computational efficiency.

4.2.1 System configuration: The test system consists of an IEEE 118-bus transmission system and three different radial distribution systems, which have 141 buses, 85 buses and 69 buses, respectively. As shown in Fig. 13, these three radial distribution systems are connected to the transmission system through buses 93, 102 and 108, respectively.

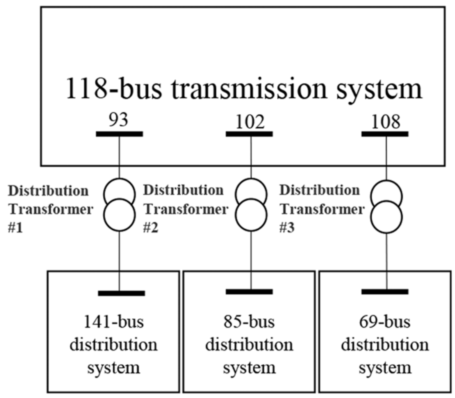

Fig. 13 *Layout of the CTDS consisting of IEEE 118-bus system and three different distribution systems*

Table 7 Parameters of the distribution systems

Distribution system	Line no.	Voltage base	P_l, MW	Q_l, Mvar
141-bus system [27]	140	12.5 kV	11.9	7.38
85-bus system [28]	84	11.0 kV	2.57	2.62
69-bus system [29]	68	12.7 kV	3.80	2.69

Table 8 Nodes with RES units installed

Distribution system	$\mathcal{N}_w$	$\mathcal{N}_{pv}$
141-bus system	20 28 32 123 125 127 129	42 65 89 94
85-bus system	10 12 15 58 63 67 70	44 47 50 52
69-bus system	13 19 23 55 58 61 69	29 34 38 44

Table 9 Cumulants of the equivalent boundary power injections in Case II

Method	Bus	$\gamma^1_{P\mathrm{eq}}$	$\gamma^2_{P\mathrm{eq}}$	$\gamma^3_{P\mathrm{eq}}$	$\gamma^4_{P\mathrm{eq}}$
PEMM	93	-0.1092	9.25×10^{-6}	1.26×10^{-9}	-1.78×10^{-12}
	102	-0.0251	4.48×10^{-7}	1.57×10^{-11}	-5.13×10^{-15}
	108	-0.0352	2.88×10^{-6}	3.53×10^{-11}	-1.50×10^{-14}
LR	93	-0.1092	6.09×10^{-6}	-5.77×10^{-9}	-1.72×10^{-11}
	102	-0.0251	3.05×10^{-7}	-5.02×10^{-11}	-7.45×10^{-14}
	108	-0.0352	1.57×10^{-6}	-2.6×10^{-10}	-1.42×10^{-12}
Method	Bus	$\gamma^1_{Q\mathrm{eq}}$	$\gamma^2_{Q\mathrm{eq}}$	$\gamma^3_{Q\mathrm{eq}}$	$\gamma^4_{Q\mathrm{eq}}$
PEMM	93	-0.0787	1.40×10^{-6}	5.57×10^{-16}	-6.09×10^{-21}
	102	-0.0280	1.58×10^{-7}	-1.06×10^{-15}	-1.41×10^{-20}
	108	-0.0280	1.20×10^{-6}	-2.21×10^{-18}	1.20×10^{-24}
LR	93	-0.0787	1.04×10^{-6}	2.32×10^{-11}	-1.48×10^{-13}
	102	-0.0280	1.07×10^{-7}	-1.87×10^{-13}	1.77×10^{-15}
	108	-0.0280	7.68×10^{-7}	1.11×10^{-11}	-1.64×10^{-13}

The detailed data of the IEEE 118-bus transmission system can be found in [23]. The parameters of the distribution systems are summarised in Table 7. The reactance of the distribution transformers is 0.05 p.u. on the base of 100 MVA.

There are multiple RES units installed in the distribution system, and the detailed installation sites are presented in Table 8, where $\mathcal{N}_w$ and $\mathcal{N}_{pv}$ represent the node sets with WFs installed and with PV plants installed, respectively. The RES penetration level, in this case, is set to 12.86%.

In this case, to investigate the applicability of PEMM on the practical RES data, the uncertainty models of RES are data based, rather than limited to the specified probability distribution. The non-parametric KDE technique is used to obtain the CDFs of the RES data. Later, the copula function is utilised to establish dependent structures. After establishing the uncertain models based on the non-parametric KDE technique and the copula function, we can obtain the relevant statistics such as moments and cumulants of RES to proceed with the PEMM. The detailed processing procedure can refer to Section 3.4. We obtain the data on wind speed and solar irradiation from the website of the National Renewable Energy Laboratory (NREL) [30].

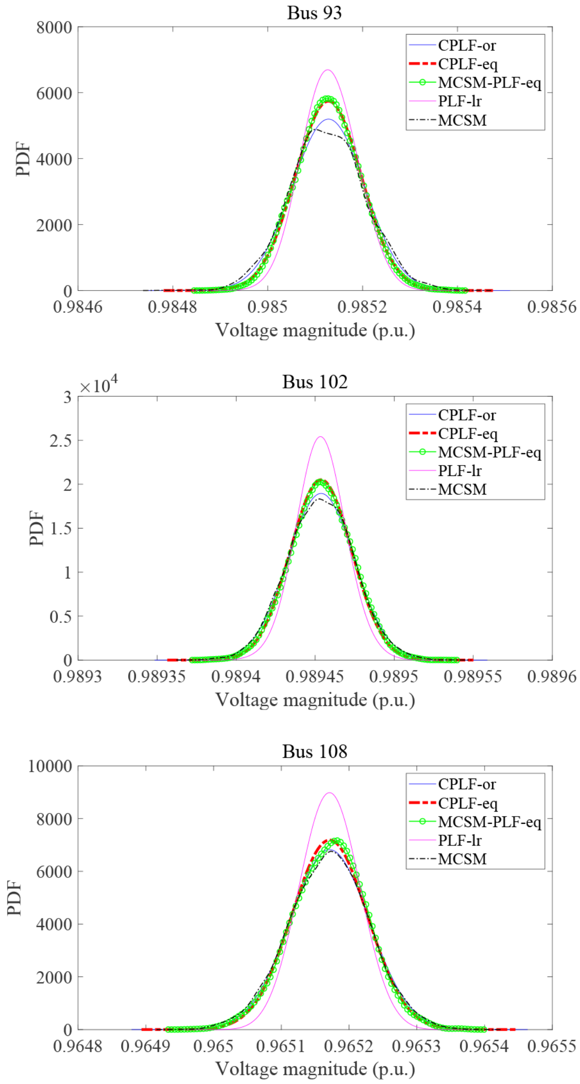

Fig. 14 *PDF curves of the voltage magnitude of boundary buses in IEEE 118-bus system*

4.2.2 Evaluation of PEMM: Applying the PEMM and the LR to construct the equivalent models, respectively, the uncertain boundary power injection can be obtained and their detailed data is shown in Table 9.

The process of accessing the accuracy of the probabilistic equivalent models in Case II is similar to that in Case I. Likewise, Figs. 14–16 depict the PDF curves of selected state variables, including the voltage magnitude of the boundary buses and the power flows of some of the branches connected to the boundary buses. Both the CPLF-eq and MCSM-PLF-eq curves are close to the MCSM and CPLF-or curves while the deviations of the PLF-lr curves are relatively significant, which verify the superiority of PEMM on the aspect of modelling accuracy.

Besides, Fig. 17 shows ARMS errors of the voltage magnitude of the boundary buses and the power flows of all the branches connected to the boundary buses in the IEEE 118-bus system. Compared with the capacity of the IEEE 118-bus system, the capacity of the three distribution systems in Case II is minor. The uncertainty in these three distribution systems cannot have a large impact on the other state variables in the IEEE 118-bus system. Hence, Fig. 17 selected the representative state variables to present. The relatively minor errors of the CPLF-eq and MCSM-PLF-eq can further substantiate the high accuracy of the equivalent model.

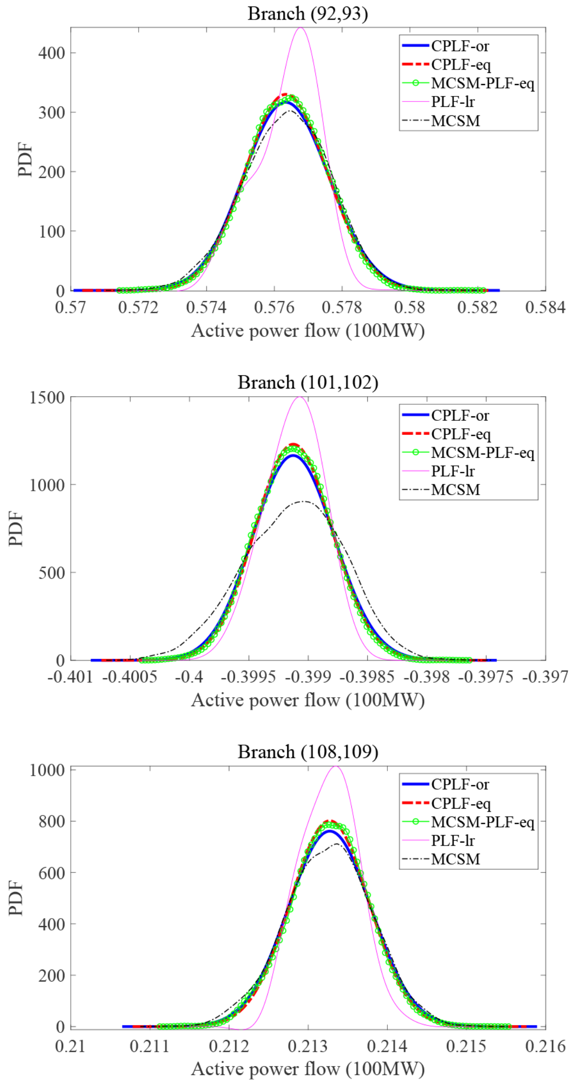

Fig. 15 *PDF curves of the active power flow of the branches connected to boundary buses in IEEE 118-bus system*

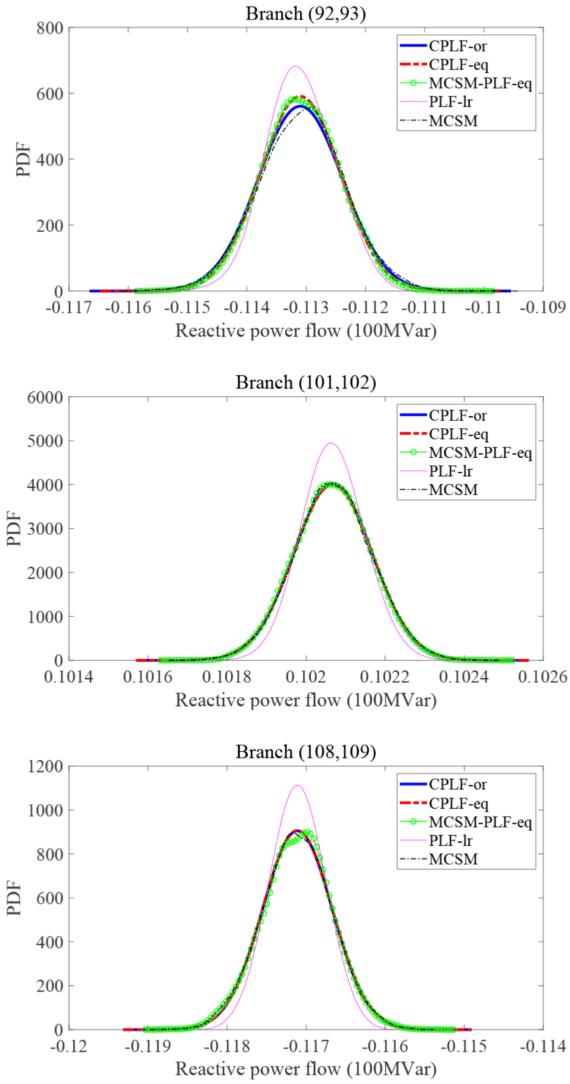

Fig. 16 *PDF curves of the reactive power flow of the branches connected to boundary buses in IEEE 118-bus system*

4.2.3 Computational efficiency: Table 10 shows the computational efficiency of different PLF algorithms and models in Case II. In addition to the main findings presented in Case I, the superiority of the PEMM in accelerating calculation is more obvious in Case II. For example, in Case I, using the equivalent model to perform the PLF algorithms on the transmission system, it can save about 81.89% of the time for the CPLF calculation and about 41.45% of the time for the MCS-PLF calculation. In Case II, using the equivalent model from PEMM to perform the PLF algorithms on the transmission system can save about 90.00% of the time for the CPLF calculation and about 71.52% of the time for the MCS-PLF calculation. It is expected that the benefit of boosting the calculation by using PEMM will be more obvious if the scale of ADN becomes large. For PEMM, building the equivalent model consumes 0.023 s and the CPLF calculation on the equivalent model only consumes 0.085 s. Thus, PEMM can facilitate some real-time applications.

4.3 Discussion

The results from Case II have shown the potential of the proposed method on accelerating the probabilistic analysis of the IEEE 118 bus system with three heterogeneous distribution systems connected. It is expected that with the expansion of the scale of the distribution systems, the superiority of the proposed method over conducting the analysis upon the whole system will be more significant. Besides, it is noted that a practical transmission system is connected to hundreds or thousands of distribution systems, supplying power to a large area. In this context, the application of the equivalent technique of distribution systems is imperative because it is computationally intractable to analyse a transmission network with detailed hundreds or thousands of distribution systems. Besides, the PLF calculation based on the equivalent method in Case II consumes only 0.085 s, which unveils the potential of the proposed method in real-time scenarios. For example, it can be applied in the real-time secure margin analysis of the power flow of the tie-line between the transmission and distribution networks. It is also promising in the online static voltage stability analysis of the transmission system considering the uncertainty of ADNs.

5 Conclusions and future work

A PEMM for ADNs considering the uncertainty of RESs is proposed in this paper. The mathematical formulation of the PEMM is investigated and extended to consider the correlations among RESs. The copula function is utilised to characterise the correlation among RES and an inverse transform sampling-based method is used to derive the joint cumulants of power injections. The case studies on two different test systems demonstrate the effectiveness and necessity of PEMM. The comparison of both the PDF curves and the ARMS errors demonstrates the superior accuracy of the PEMM compared to the LR method. The PLF results of the equivalent model obtained from the PEMM are in good agreement with those of the original model. The simulation results on a test system consisting of IEEE 118-bus system and three different distribution system shows the potential of PEMM on expediting the PLF calculations of the transmission system. It is

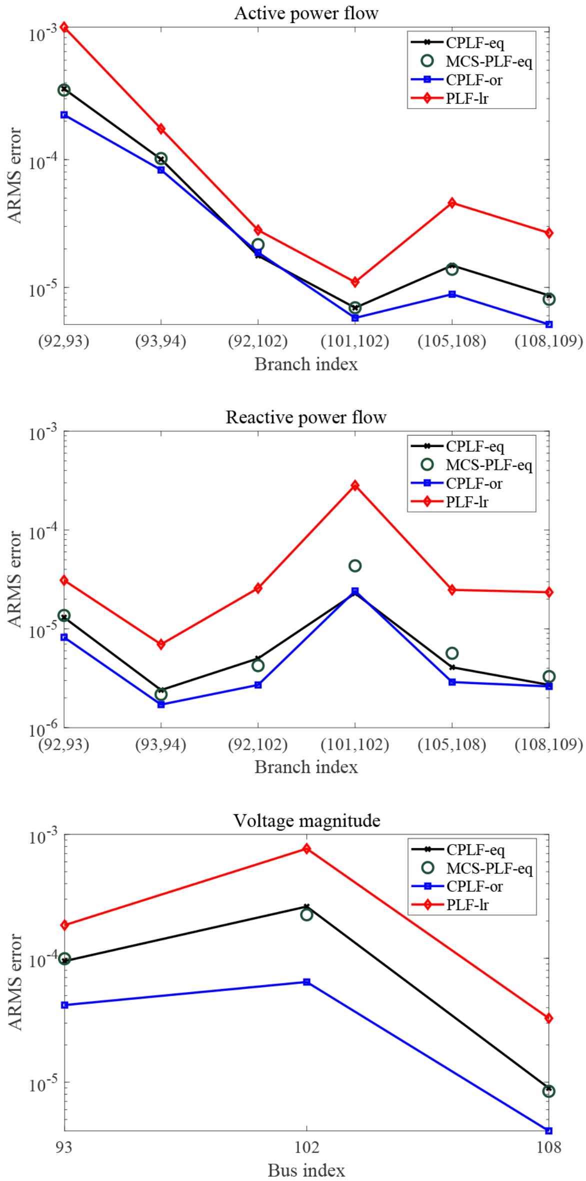

Fig. 17 *ARMS error of active power flow, reactive power flow and voltage magnitude of the boundary buses and their connected branches in the IEEE 118-bus system*

Table 10 Computational efficiency of different PLF algorithms and models in Case II

	t_m, s	t_c, s	n_{var}
MCSM	-	97.155	1733
CPLF-or	-	1.080	1733
PLF-lr	0.371	0.067	553
CPLF-eq	**0.023**	**0.085**	553
MCS-PLF-eq	**0.023**	**27.670**	553

reported that PEMM can save about 90.00% of the time for the CPLF calculation and about 71.52% of the time for the MCS-PLF calculation.

The proposed PEMM can be used to provide the equivalent model for applications in transmission networks in which one should consider the impact of RES. For example, PEMM can be exploited to solve some real-time problems such as the real-time secure margin analysis of the power flow of the tie-line between the transmission and ADNs. Furthermore, the multi-linearisation technique can be developed to tackle the voltage-related errors in PEMM.

6 Acknowledgments

This work was supported in part by the National Natural Science Foundation of China under Grant 51807066, the Guangdong Basic and Applied Basic Research Foundation under Grant 2019A1515011408, the Science and Technology Program of Guangzhou under Grant 201904010215 and the Talent Recruitment Project of Guangdong under Grant 2017GC010467.

7 References

[1] Adefarati, T., Bansal, R.C.: 'Integration of renewable distributed generators into the distribution system: a review', *IET Renew. Power Gener.*, 2016, **10**, (7), pp. 873–884

[2] Ehsan, A., Cheng, M., Yang, Q.: 'Scenario-based planning of active distribution systems under uncertainties of renewable generation and electricity demand', *CSEE J. Power Energy Syst.*, 2019, **5**, (1), pp. 56–62

[3] Sannigrahi, S., Ghatak, S., Acharjee, P.: 'Multi-objective optimisation-based active distribution system planning with reconfiguration, intermittent RES, and DSTATCOM', *IET Renew. Power Gener.*, 2019, **13**, (13), pp. 2418–2429

[4] Dai, W., Yu, J., Liu, X., *et al.*: 'Two-tier static equivalent method of active distribution networks considering sensitivity', *Int. J. Electr. Power Energy Syst.*, 2018, **100**, pp. 193–200
[5] Zali, S., Milanović, J.: 'Generic model of active distribution network for large power system stability studies', *IEEE Trans. Power Syst.*, 2013, **28**, (3), pp. 3126–3133
[6] Milanović, J., Zali, S.: 'Validation of equivalent dynamic model of active distribution network cell', *IEEE Trans. Power Syst.*, 2012, **28**, (3), pp. 2101–2110
[7] Golpîra, H., Seifi, H., Haghifam, M.: 'Dynamic equivalencing of an active distribution network for large-scale power system frequency stability studies', *IET. Gener. Transm. Distrib.*, 2015, **9**, (15), pp. 2245–2254
[8] Samadi, A., Söder, L., Shayesteh, E., *et al.*: 'Static equivalent of distribution grids with high penetration of PV systems', *IEEE Trans. Smart Grid*, 2015, **6**, (4), pp. 1763–1774
[9] Jeong, M., Kim, Y., Moon, S., *et al.*: 'Optimal voltage control using an equivalent model of a low-voltage network accommodating inverter-interfaced distributed generators', *Energies*, 2017, **10**, (8), p. 1180
[10] Neto, A., Rodrigues, A., Prada, R., *et al.*: 'External equivalent for electric power distribution networks with radial topology', *IEEE Trans. Power Syst.*, 2008, **23**, (3), pp. 889–895
[11] Baziar, A., Kavousi-Fard, A.: 'Considering uncertainty in the optimal energy management of renewable micro-grids including storage devices', *Renew. Energy*, 2013, **59**, pp. 158–166
[12] Xie, Z., Ji, T., Li, M., *et al.*: 'Quasi-Monte Carlo based probabilistic optimal power flow considering the correlation of wind speeds using copula function', *IEEE Trans. Power Syst.*, 2017, **33**, (2), pp. 2239–2247
[13] Li, M., Lin, Z., Ji, T., *et al.*: 'Risk constrained stochastic economic dispatch considering dependence of multiple wind farms using pair-copula', *IEEE Trans. Power Syst.*, 2018, **226**, pp. 967–978
[14] Usaola, J.: 'Probabilistic load flow with wind production uncertainty using cumulants and cornish–fisher expansion', *Int. J. Electr. Power Energy Syst.*, 2009, **31**, (9), pp. 474–481
[15] Kumar, K., Saravanan, B.: 'Recent techniques to model uncertainties in power generation from renewable energy sources and loads in microgrids–a review', *Renew. Sust. Energy Rev.*, 2017, **71**, (9), pp. 348–358
[16] Morales, J., Perez-Ruiz, J.: 'Point estimate schemes to solve the probabilistic power flow', *IEEE Trans. Power Syst.*, 2007, **22**, (4), pp. 1594–1601
[17] Kendall, M.G.: '*The advanced theory of statistics*' (Charles Griffin and Co., Ltd, 1946, 2nd edn.)
[18] Morales, J., Baringo, L., Conejo, A., *et al.*: 'Probabilistic power flow with correlated wind sources', *IET. Gener. Transm. Distrib.*, 2010, **4**, (5), pp. 641–651
[19] Sklar, A.: 'Random variables, joint distribution functions, and copulas', *Kybernetika*, 1973, **9**, (6), pp. 449–460
[20] Bouye, E., Durrleman, V., Nikeghbali, A., *et al.*: 'Copulas for Finance - A Reading Guide and Some Applications', 2000, Available at SSRN 1032533
[21] Thomas, W.: 'A new technique for maximum-likelihood canonical Gaussian ordination', *Ecolog. Monogr.*, 2004, **74**, (4), pp. 685-–701
[22] Geweke, J.: 'Efficient simulation from the multivariate normal and student-t distributions subject to linear constraints and the evaluation of constraint probabilities'. Proc. the 23rd Symp. on the Interface, Virginia, USA, 1991, pp. 571–578
[23] Zimmerman, R., Murillo-Sánchez, C., Thomas, R.J.: 'MATPOWER: steady-state operations, planning, and analysis tools for power systems research and education', *IEEE Trans. Power Syst.*, 2010, **26**, (1), pp. 12–19
[24] Zhang, P., Lee, S.: 'Probabilistic load flow computation using the method of combined cumulants and gram-charlier expansion', *IEEE Trans. Power Syst.*, 2004, **19**, (1), pp. 676–682
[25] Williams, T., Crawford, C.: 'Probabilistic load flow modeling comparing maximum entropy and gram-charlier probability density function reconstructions', *IEEE Trans. Power Syst.*, 2012, **28**, (1), pp. 272–280
[26] Debs, A.: 'Estimation of external network equivalents from internal system data', *IEEE Trans. Power Appar. Syst.*, 1975, **94**, (2), pp. 273–279
[27] Khodr, H.M., Olsina, F.G., De Oliveira-De Jesus, P.M., *et al.*: 'Maximum savings approach for location and sizing of capacitors in distribution systems', *Electr. Power Syst. Res.*, 2008, **78**, (7), pp. 1192–1203
[28] Das, D., Kothari, D.P., Kalam, A.: 'Simple and efficient method for load flow solution of radial distribution networks', *Int. J. Electr. Power Energy Syst.*, 1995, **17**, (5), pp. 335–346
[29] Das, D.: 'Optimal placement of capacitors in radial distribution system using a fuzzy-GA method', *Int. J. Electr. Power Energy Syst.*, 2008, **30**, (6-7), pp. 361–367
[30] 'NERL - Renewable Resource Data', Available at https://www.nrel.gov/grid/solar-resource/renewable-resource-data.html, accessed 10 December 2019.